Mid-Holocene ENSO: Issues in quantitative model-proxy data comparisons

J. Brown,[1,2] A. W. Tudhope,[3] M. Collins,[4] and H. V. McGregor[5,6]

Received 28 June 2007; revised 17 January 2008; accepted 21 April 2008; published 9 July 2008.

[1] Evaluation of climate model simulations using observed data contributes to the assessment of confidence in model predictions of future climate change. The mid-Holocene represents an opportunity to evaluate model simulations of El Niño–Southern Oscillation (ENSO) in comparison with coral proxy evidence of reduced ENSO amplitude. Quantitative comparisons between coral records and model output have been limited by (1) the use of different measures of ENSO amplitude, (2) possible sampling of natural variability in short records, and (3) uncertainty about the stationarity of the relationship between central Pacific sea surface temperature (SST) variability and ENSO signals at the coral site. We examine these issues using modern and fossil coral records from the western Pacific and model simulations of preindustrial and mid-Holocene climate. As a measure of ENSO amplitude, the standard deviation is found to be preferable to event frequency or size as event-based measures are highly dependent on the choice of threshold and may be unreliable for a small number of events. Model ENSO amplitude is found to be strongly dependent on the choice of averaging period, with calendar year averages smoothing the seasonal ENSO signal. A relatively robust relationship between SST variability in the NINO3.4 region and the ENSO SST and precipitation anomalies archived in corals is demonstrated for the instrumental period and for a set of model simulations. Remaining uncertainty about changes in ENSO teleconnections under paleoclimate conditions implies the need for additional proxy records from ENSO-sensitive regions before quantitative reconstructions of ENSO amplitude can be used to evaluate model sensitivity.

Citation: Brown, J., A. W. Tudhope, M. Collins, and H. V. McGregor (2008), Mid-Holocene ENSO: Issues in quantitative model-proxy data comparisons, *Paleoceanography*, *23*, PA3202, doi:10.1029/2007PA001512.

1. Introduction

[2] There is increasing interest in the use of paleoclimate reconstructions to evaluate the ability of models to simulate a range of climate conditions and to weight models or model versions in the construction of probabilistic future projections [e.g., *Collins et al.*, 2006; *Brown et al.*, 2008]. The response of El Niño–Southern Oscillation (ENSO) to mid-Holocene (6000 years before present (6 ka)) conditions represents one test of model ENSO sensitivity to climate forcing. Reconstructions of tropical interannual variability from proxy records such as coral and lake sediment cores suggest that ENSO was substantially weaker at this time in response to orbitally driven changes in the seasonal cycle of insolation. In order to carry out quantitative model-data comparisons, the target for model simulations must be well defined. In previous studies of mid-Holocene ENSO, different measures of ENSO amplitude have been used for models and proxy records, resulting in ambiguity about the ability of models to reproduce the magnitude of weakening of ENSO inferred from proxy records.

[3] This study aims to compare several different measures of ENSO amplitude employed in previous studies: the number of El Niño events over a threshold, the standard deviation of interannual variability, the average size of El Niño events, and the average size of the largest El Niño events in order to determine which is the most robust measure for both coral records and models. We compare the mid-Holocene change in ENSO amplitude reconstructed from two sets of coral records from Papua New Guinea (PNG) to the change simulated by the third version of the Hadley Centre coupled model (HadCM3) using the different measures and discuss the implications for quantitative model-data comparison studies. We also quantify the expected change in local tropical western Pacific precipitation and sea surface temperature (SST) variability associated with ENSO for a given change in tropical central Pacific SST variability. The relationship is investigated using observations and modern coral records from the instrumental period as well as a set of climate simulations performed using different versions of HadCM3 with a wide range of ENSO characteristics. We conclude with a discussion of the

[1]Department of Meteorology, University of Reading, Reading, UK.
[2]Now at School of Geography and Environmental Science, Monash University, Clayton, Victoria, Australia.
[3]School of Geosciences, University of Edinburgh, Edinburgh, UK.
[4]Hadley Centre for Climate Prediction and Research, Met Office, Exeter, UK.
[5]School of Earth and Environmental Sciences, University of Wollongong, Wollongong, New South Wales, Australia.
[6]Institute of Environmental Research, Australian Nuclear Science and Technology Organisation, Menai, New South Wales, Australia.

0883-8305/08/2007PA001512$12.00

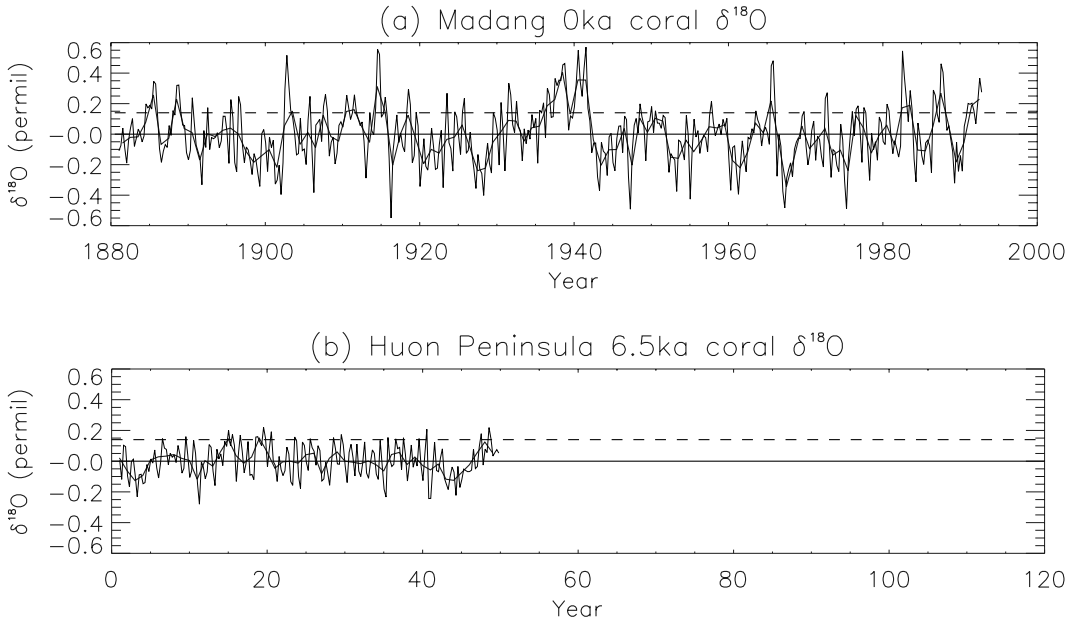

Figure 1. $\delta^{18}O$ from (a) modern coral from Madang, Papua New Guinea, and (b) mid-Holocene (6.5 ka) fossil coral from Huon Peninsula, Papua New Guinea. From *Tudhope et al.* [2001]. Adapted with permission from AAAS. Coral $\delta^{18}O$ are annual averages (thick line) and seasonal averages (thin line) with mean and linear trend removed. Annual average values are based on calendar years. Dashed line indicates the +0.14‰ threshold for modern El Niño events.

implications for reconciling model simulations and coral proxy records of mid-Holocene ENSO.

2. Coral Records of Mid-Holocene ENSO

[4] In order to reconstruct paleo-ENSO, annually or subannually resolved proxy records of SST, salinity, or precipitation from regions with a strong ENSO climate signal are required. Coral and laminated lake sediments provide the majority of multidecadal, high-resolution records suitable for reconstructing ENSO variability over the Holocene. Lake sediment records from southern Ecuador and the Galápagos Islands have been interpreted as showing that heavy precipitation associated with moderate to strong El Niño events was reduced in frequency during the early Holocene to mid-Holocene [*Rodbell et al.*, 1999; *Moy et al.*, 2002; *Riedinger et al.*, 2002]. Coral records potentially include information about both weak and strong ENSO events and are therefore more readily compared with a continuous time series of ENSO activity from climate model simulations.

[5] This study focuses on two sets of previously published coral records from the north coast of PNG [*Tudhope et al.*, 2001; *McGregor and Gagan*, 2004], located in the western center of action of ENSO in the western Pacific warm pool. These records have been used to reconstruct changes in ENSO from the interannual variability of oxygen isotope ratios ($\delta^{18}O$) in mid-Holocene fossil corals compared to modern corals from the same sites. Oxygen isotope records at both sites represent changes in SST and the $\delta^{18}O$ of seawater, which reflects changes in sea surface salinity and freshwater input into the nearshore marine environment. The relevant results from the studies of *Tudhope et al.* [2001] and *McGregor and Gagan* [2004] are summarized below.

[6] *Tudhope et al.* [2001] used fossil coral oxygen isotope records from the Huon Peninsula, PNG, to obtain records of tropical climate for several time slices during the Holocene, which were compared with living corals from sites at Huon Peninsula, Madang, and Laing Island. The oxygen isotope ratios in the modern corals were found to be strongly correlated with ENSO activity due to cooler (warmer) SSTs and decreased (increased) precipitation during El Niño (La Niña) events. Modern coral records were demonstrated to have significant coherence with instrumental ENSO indices and to reproduce changes in ENSO amplitude over the instrumental period [*Tudhope et al.*, 1995, 2001].

[7] The 6.5 ka (mid-Holocene) fossil coral record is 49 years long, with 12 samples per year averaged into four seasonal oxygen isotope ratio values (corresponding approximately to December–February, March–May, etc.). ENSO variability was analyzed using 2.5–7 year band-pass-filtered seasonal data. The Madang modern coral record and the Huon Peninsula 6.5 ka fossil coral record are shown in Figure 1. The oxygen isotope ratios in the mid-Holocene fossil coral have reduced variability on ENSO timescales of up to 60% compared to the variability in modern records, calculated from the standard deviation of the 2.5–7 year band-pass-filtered seasonal isotopic values [*Tudhope et al.*, 2001]. The standard deviation of interannual oxygen isotope ratio variability measures both El Niño and La Niña events archived in the coral isotopic record.

[8] *McGregor and Gagan* [2004] obtained mid-Holocene fossil coral records from Koil and Muschu islands, offshore

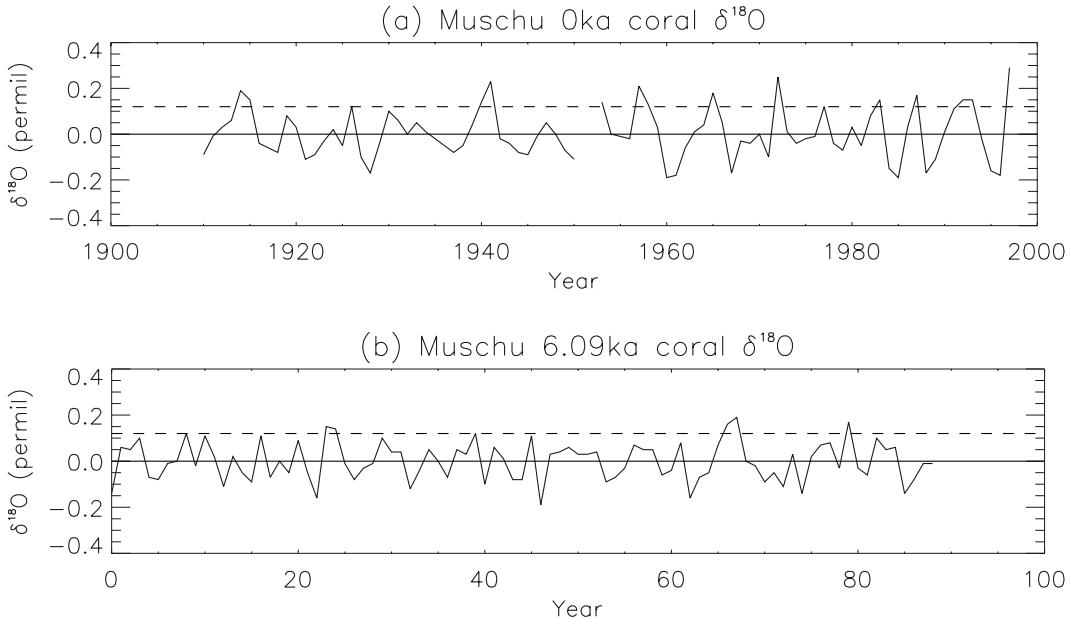

Figure 2. δ^{18}O from (a) modern and (b) mid-Holocene (6.09 ka) fossil coral from Muschu Island, Papua New Guinea, adapted from *McGregor and Gagan* [2004]. Coral δ^{18}O are annual averages with 10 year running mean subtracted. Annual average values are based on approximate calendar years. Dashed line indicates the +0.12‰ threshold for modern El Niño events.

from the Sepik River on the north coast of PNG. Seven fossil coral records were analyzed from the period 7.6–5.4 ka, ranging in length from 9 to 89 years. Annual average oxygen isotope ratios were used to investigate changes in interannual variability, with the year defined from approximately January to December, following the annual cycle of density banding in the coral. The fossil coral records were compared to a modern record of 86 years in length (1910–1997 with 2 years missing), shown in Figure 2. The frequency and amplitude of El Niño events were calculated for events above the δ^{18}O anomaly threshold of +0.12‰, defined from the magnitude of isotopic anomalies associated with El Niño events in the modern record. The modern record was found to capture 14 out of 16 observed El Niño events in the period 1910–1997 (a frequency of 16 events per century), in comparison to the observational record compiled by *Trenberth* [1997].

[9] Using the same threshold of +0.12‰ isotope anomaly for all records, the frequency of events was found to be reduced from 16 per century in the modern coral to 12 and 8 events per century for the 7.6–7.1 and 6.1–5.4 ka corals, respectively [*McGregor and Gagan*, 2004]. The average El Niño amplitude was calculated from the average isotope anomaly for all events above the threshold in the modern and fossil coral records. The average amplitude of mid-Holocene El Niño events was 15% less than the average amplitude of modern events by this measure. As the use of an absolute threshold results in fewer events being identified in the mid-Holocene records than the modern record, the change in El Niño event frequency found by *McGregor and Gagan* [2004] may be at least partially due to the reduced amplitude of events; that is, El Niño events occur in the weak to moderate band, which was not analyzed in that study. Changes in La Niña events (negative oxygen isotope anomalies) were not considered.

3. Model Simulations of Mid-Holocene ENSO

[10] Previous model simulations of tropical climate and ENSO variability over the Holocene include the Zebiak-Cane model simulations of *Clement et al.* [2000, 2001] as well as a range of global climate model (GCM) simulations [e.g., *Hewitt and Mitchell*, 1998; *Bush*, 1999; *Liu et al.*, 2000; *Kitoh and Murakami*, 2002; *Otto-Bliesner et al.*, 2003; *Brown et al.*, 2006a, 2008]. Reduced complexity models (such as the Zebiak-Cane model) have the advantage that they may be run for many thousands of years of simulation to produce robust climate signals, but they may suffer from missing or incomplete feedback loops because of the simplification of some physical processes and limited spatial domain. Global climate models attempt to represent all important physical processes (with varying degrees of success) but as a consequence are much more expensive to run and can only produce a limited number of simulation years (of the order of several hundred years). Intermediate models, such as the Fast Ocean Atmosphere Model (FOAM) used by *Liu et al.* [2000], are designed to achieve a compromise between complexity and computational cost.

[11] The model simulations were forced with changes in insolation resulting from orbital variations as well as changes in atmospheric composition and vegetation distribution in some cases. Consistent responses to mid-Holocene forcing in all coupled model simulations include a strengthening of the Asian and North African summer monsoons [e.g., *Liu et al.*, 2004; *Braconnot et al.*, 2007]. Changes in ENSO in the mid-Holocene have been investigated in a

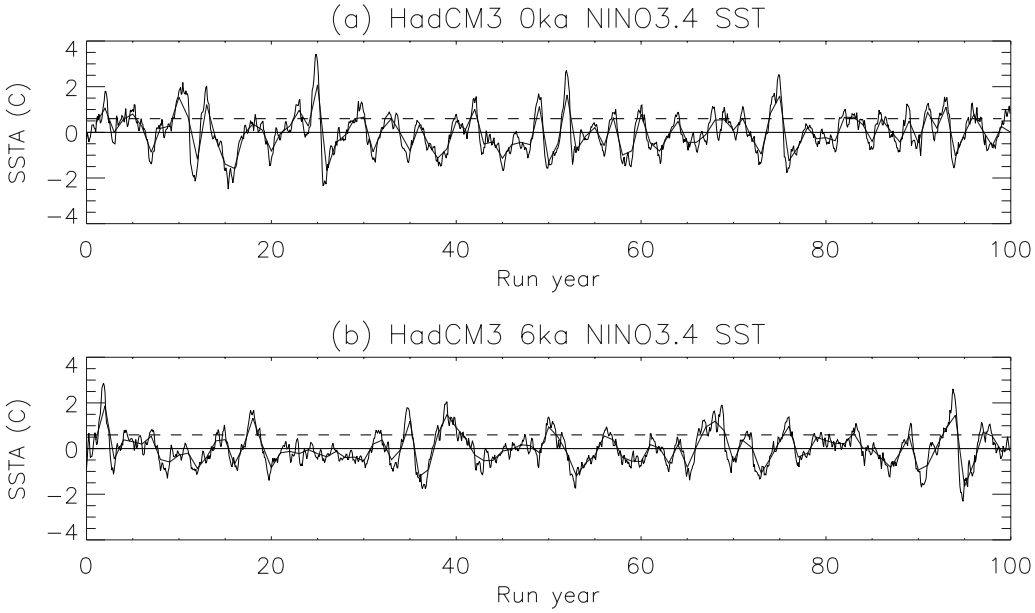

Figure 3. HadCM3 standard model NINO3.4 SST anomalies from (a) preindustrial and (b) mid-Holocene (6 ka) simulations. SST anomalies are July–June annual averages (thick line) and monthly values (thin line). Dashed line indicates the +0.57°C threshold for modern El Niño events.

subset of studies [e.g., *Clement et al.*, 2000; *Liu et al.*, 2000; *Otto-Bliesner et al.*, 2003; *Brown et al.*, 2006a], using a variety of measures of ENSO amplitude and event frequency.

[12] The Zebiak-Cane model study of *Clement et al.* [2000] measured changes in ENSO amplitude from the number of El Niño events over a threshold of +3°C for December–January–February average SST anomalies in the NINO3 region (5°N–5°S, 90°W–150°W) as well as the average magnitude of events over this threshold. The FOAM modeling study of *Liu et al.* [2000] calculated the change in average El Niño and La Niña SST anomalies in the NINO3.4 region (5°N–5°S, 120°W–170°W) using the 10 strongest warm and cold events from 120 year model runs and calculating the change in variance in the ENSO frequency band from the NINO3.4 SST anomaly power spectrum. The National Center for Atmospheric Research Climate System Model study of *Otto-Bliesner et al.* [2003] and the HadCM3 study of *Brown et al.* [2008] measured ENSO amplitude change from the standard deviation of monthly NINO3 SST anomalies. While these studies found different changes in ENSO frequency in the mid-Holocene, all found a reduction in ENSO amplitude of the order of 5–20%, according to the various measures employed.

[13] Simulations of mid-Holocene and preindustrial climate have been carried out with the standard version of HadCM3 as well as model versions with different configurations of ocean heat and salinity flux adjustments and perturbed model parameter settings [*Collins et al.*, 2006; *Brown et al.*, 2006a, 2008; *Toniazzo et al.*, 2008]. In this study, we first consider the standard model simulations of preindustrial and mid-Holocene climate. In order to explore a wider range of model ENSO variability, we then make use of a set of simulations carried out with versions of HadCM3 for which selected parameters in the atmospheric model are perturbed within a plausible, expert-defined range [*Murphy et al.*, 2004; *Collins et al.*, 2006]. A total of 34 "perturbed physics" coupled model versions were used to simulate preindustrial climate, while a subset of four of these model versions was also used to simulate mid-Holocene climate. In order to prevent model drift, ocean heat and salinity flux adjustments were used in the perturbed physics simulations, reducing some climatological biases present in the standard model version, as discussed by *Brown et al.* [2008].

[14] The standard model simulations consist of 100-year runs with different orbital forcing for preindustrial and mid-Holocene climate and a constant atmospheric composition and land surface configuration [*Brown et al.*, 2006a, 2008]. In these simulations, the standard deviation of preindustrial monthly NINO3 SST anomalies is 0.81°C, while the standard deviation of mid-Holocene monthly NINO3 SST anomalies is 0.71°C (a 12% reduction in amplitude). A similar result is found using monthly NINO3.4 SST anomalies (0.86°C for preindustrial and 0.74°C for mid-Holocene, a 14% reduction), as shown in Figure 3. As in previous studies, we consider it appropriate to compare the NINO3 or NINO3.4 SST variability from the coupled model with proxy records which respond to ENSO signals in SST and precipitation elsewhere (in this case, in the western Pacific warm pool). While the use of local measures of ENSO variability at the proxy site would constitute a more direct comparison, such a comparison is complicated by biases in the simulation of ENSO teleconnections by the model, as discussed further in section 5.

4. Comparison of Measures of ENSO Amplitude

[15] The amplitude of ENSO variability in the coral records and model simulations was calculated using the

Table 1. Amplitude of ENSO in Modern and Mid-Holocene Coral and Preindustrial and Mid-Holocene HadCM3 Standard Model Simulations, as Calculated From Coral $\delta^{18}O$ and Model NINO3.4 SST Anomalies[a]

	Number of Years	Events per Century[b]	Annual Standard Deviation	Average of All Events	Average of 10 Largest Events
Coral Record					
Madang 0 ka coral	112	16 (18)	0.14	0.23	0.29
Huon Peninsula 6.5 ka coral	49	4 (2)	0.06	0.15	–
Muschu Island 0 ka coral	86	16 (14)	0.11	0.18	0.23[c]
Muschu Island 6.09 ka coral	89	6 (5)	0.08	0.16	0.16[c]
Model Run					
HadCM3 0 ka run	100	16	0.64	0.90	1.07
HadCM3 6 ka run	100	18	0.62	0.97	1.19
HadCM3 0 ka run[d]	100	25	0.75	0.95	1.33
HadCM3 6 ka run[d]	100	15	0.64	1.07	1.23

[a]Coral $\delta^{18}O$ is given per mil, and model NINO3.4 SST is given in degrees Celsius. All analysis is for calendar year annual averages unless specified.
[b]Event frequency scaled to events per century to facilitate comparison. Actual number of events given in parentheses.
[c]Five largest events only.
[d]Averages from July–June.

number of El Niño events above a threshold per century, the standard deviation of interannual variability, the average El Niño event size, and the average size of the largest El Niño events. The longest-available modern and mid-Holocene coral records were used from each of the PNG sites, consisting of a 112-year modern coral record from Madang, a 49 year fossil coral record from the Huon Peninsula [*Tudhope et al.*, 2001], and an 86 year modern coral record and an 89 year fossil coral record from Muschu Island [*McGregor and Gagan*, 2004]. While multiple mid-Holocene records are available from Muschu Island, we use only the single longest record as the primary aim of this study is to explore issues in proxy data-model intercomparison rather than to estimate ENSO amplitude from coral or models. The seasonal Huon Peninsula and Madang coral records are converted to (calendar year) annual average values to facilitate comparison with the annual average Muschu Island coral oxygen isotope values.

[16] To calculate the number and size of El Niño events, we adopt a method consistent with that of *McGregor and Gagan* [2004] and define an El Niño event as an oxygen isotope anomaly exceeding a threshold of +0.12‰ for the Muschu Island coral records. This results in 16 El Niño events per century for the modern coral; therefore a threshold is adopted for the coral records of *Tudhope et al.* [2001] which results in the same number of events in the modern Madang coral. The threshold required to produce 16 events per century in the modern Madang coral is an isotope anomaly of +0.14‰ because of the larger amplitude of variability in this coral record. La Niña events (negative oxygen isotope anomalies) are not considered in the calculation of event size.

[17] The threshold for El Niño events in the model simulations is a NINO3.4 SST anomaly of +0.57°C, resulting in the same number of El Niño events per century as the coral records (16 events per century, or 16 El Niño years out of the 100 year model run). *McGregor and Gagan* [2004] compared their modern coral with the observational ENSO record of *Trenberth* [1997], who defined an El Niño event on the basis of the 5 month running mean NINO3.4 SST anomalies exceeding +0.4°C for 6 months. The definition is modified in this study to consider annual average NINO3.4 SST anomalies to allow comparison with the annual average coral records.

[18] For each coral record, the ENSO amplitude calculated using each of the four measures is shown in Table 1. The percentage change from modern time to the mid-Holocene for each measure of ENSO amplitude is given in Table 2. There is a reduction of more than 60% in the mid-Holocene in the number of El Niño events per century for both sets of corals. Using the standard deviation of annual average isotope anomalies to define ENSO amplitude, the amplitude is reduced by 57% in the mid-Holocene coral from Huon Peninsula compared to the modern coral from Madang, while the amplitude is reduced by 27% in the mid-Holocene coral from Muschu Island compared to the modern record. When the average of all El Niño events over a threshold is used to define ENSO amplitude, the amplitude is reduced by 35% in the Huon Peninsula mid-Holocene record and 11% in the Muschu Island mid-Holocene record compared to the modern records (consistent with the reduction of 15 ± 12% reported by *McGregor and Gagan* [2004] for a composite mid-Holocene record). As only two El Niño events are identified in the Huon Peninsula mid-Holocene coral, it is not meaningful to calculate the average of the largest events. The average of the five largest events is calculated for the Muschu Island fossil and modern coral records, with the average large event in the mid-Holocene record being 30% weaker than the average large event in the modern record. It is evident from this comparison that the choice of measure of ENSO amplitude in coral records results in widely varying estimates of changes in mid-Holocene ENSO amplitude.

[19] Changes in number of events for the different coral sites are not compared because of the extremely small number of events in the mid-Holocene Huon Peninsula coral record. When using the standard deviation or average event size, the percentage change in mid-Holocene variability in the Muschu Island coral records is less than half the change seen in the Huon Peninsula–Madang coral records.

Table 2. Percentage Change From the Modern or Preindustrial to the Mid-Holocene Period for Each Measure of ENSO Amplitude Given in Table 1

	Percent Change Events per Century	Percent Change Standard Deviation[a]	Percent Change Average Event	Percent Change Large Event
Coral Record				
Madang-Huon corals	−75	**−57**	−35	—
Muschu Island corals	−63	**−27**	−11	−30
Model Run				
HadCM3 (calendar year)	+13	−3	+8	+11
HadCM3 (July–June year)	−40	**−15**	+13	−8

[a]Changes in bold are statistically significant at the 95% confidence level (for coral) and the 90% confidence level (for model) according to an *F* test.

This may be a reflection of the different El Niño and La Niña signals at the sites, with the Muschu Island coral being more strongly influenced by freshwater inputs from the Sepik River [*Ayliffe et al.*, 2004]. There may also have been a change in the strength of ENSO between the period of the Huon coral (6.5 ka) and the Muschu coral (6.09 ka). We note that the percentage change in the standard deviation for each coral record is approximately twice as large as the percentage change in the average El Niño event isotope anomaly, which is consistent with the standard deviation recording information about both cold and warm ENSO events.

[20] The four different measures of ENSO amplitude were also compared for the preindustrial and mid-Holocene HadCM3 simulations (Tables 1 and 2). NINO3.4 SST anomalies were averaged over the calendar year (January–December) and over the year centered on boreal winter (July–June). There is an increase in the number of events per century in the mid-Holocene run of 13% when calendar year averages are used and a reduction of 40% when using July–June annual averages. The standard deviation of NINO3.4 SST anomalies is reduced in the mid-Holocene run by 3% for calendar year averages and by 15% for July–June averages (compared to a 14% reduction in the standard deviation of monthly anomalies). The average event size is increased in the mid-Holocene case for both sets of annual averages, while the mid-Holocene average of the 10 largest events is increased by 11% for calendar year averages and reduced by 8% for July–June averages.

[21] The dependence on averaging period reflects the strong seasonal phase locking of the HadCM3 ENSO signal, as discussed by *Brown et al.* [2006a]. When calendar year averages are used, the amplitudes of events are smoothed, as indicated by the greater number of events identified in the preindustrial simulation using July–June averages for a constant SST anomaly threshold. The model simulates a strong mid-Holocene reduction in the amplitude of ENSO-related SST anomalies toward the end of the calendar year, representing a damping of the peak of El Niño events in particular, in agreement with other modeling studies [e.g., *Clement et al.*, 2000]. However, when calendar year averages are used, this change in mid-Holocene ENSO amplitude is also smoothed, in this case giving a larger number of events in the mid-Holocene simulation than the preindustrial simulation (despite reduced standard deviation of annual and monthly anomalies). The various measures of ENSO amplitude were not found to be strongly dependent on averaging period in the case of the Madang and Huon Peninsula coral records (mid-Holocene coral variability is 45% less than modern coral variability when the standard deviations of seasonal anomalies are compared). This may be due to the different seasonal timing of events in the western Pacific warm pool, where El Niño events result in a reduction in precipitation and cool SST anomalies from the austral winter onward [e.g., *Tudhope et al.*, 1995; *Cane et al.*, 2000].

[22] In summary, the choice of measure of ENSO amplitude results in substantial differences in the estimate of mid-Holocene ENSO changes, including the sign of the change in some cases. The number of events, average event size, and average size of largest events are all highly dependent on the choice of threshold and are potentially dependent on changes in the proportion of strong and weak events. In addition, when records are short, too few events may be identified to give a reliable estimate of changes in frequency or amplitude. For these reasons, we find that the standard deviation of anomalies in the coral $\delta^{18}O$ or model NINO3.4 time series provides a more robust measure of ENSO amplitude than the other measures considered here. Using the standard deviation of annual averages, the coral records show a reduction in mid-Holocene ENSO amplitude of 57% and 27%, respectively, while the model simulates a much smaller reduction of only 3% for calendar year averages or 15% for July–June averages. The model estimates therefore lie outside the range of the coral reconstructions of mid-Holocene ENSO amplitude change, even when a consistent averaging period and measure of amplitude are used.

[23] An additional consideration is the statistical significance of changes in ENSO amplitude when compared with natural variability for coral or instrumental records or with model internal variability. The significance of changes in standard deviation was estimated using an *F* test (with the degrees of freedom reduced to account for autocorrelation), as indicated in Table 2. The reduction in mid-Holocene coral ENSO amplitude was found to be significant at the 95% confidence level for both sets of corals. The 3% reduction in standard deviation in the 6 ka model run using calendar year average values was not significant, while the 15% reduction using July–June averages was significant at the 92% confidence level. The internal variability of ENSO amplitude in the model was estimated using a 2000 year HadCM3 simulation of preindustrial climate [*Collins et al.*,

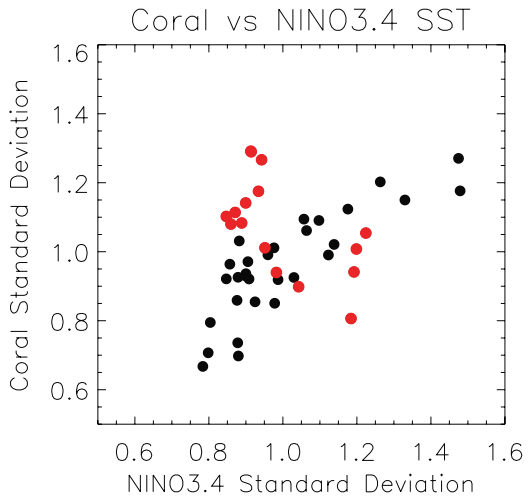

Figure 4. ENSO variability in modern Madang coral $\delta^{18}O$ and observed (HadISST) NINO3.4 SST from 1881 to 1992: normalized standard deviations of 2.5–7 year band-pass-filtered seasonal anomalies divided into 20 year sections with 2 year offset. Pre-1920 data (20 year segment midpoints from 1891 to 1910) are shown as red dots; post-1920 data are shown as black dots.

2001]. Taking overlapping 100 year segments from the 2000 year model run, with an offset of 10 years between segments, the standard deviation of seasonal NINO3 SST anomalies varied by up to ±20% (NINO3.4 SST was not available). For a smaller window length of 20 years, a larger range of NINO3 standard deviations of ±40% was calculated. Hence longer records provide more confidence in rejecting internal variability as the explanation for relatively small changes in ENSO amplitude between model runs or coral records.

5. Relationship Between Coral Records and NINO Index Variability

[24] The disagreement between the significant reductions in mid-Holocene ENSO amplitude implied by coral records and the more modest reductions simulated by coupled climate models does not appear to be due to the use of inconsistent measures of ENSO amplitude. We therefore consider whether it is valid to assume that the amplitude of ENSO-related variability of SST and precipitation at the western Pacific coral sites will vary with the same magnitude as variability in the central Pacific NINO3.4 SST used to define the model ENSO signal. In particular, the relationship between the amplitude of the two signals may alter with shifts in climate, such as changes in local western Pacific ENSO precipitation teleconnections [e.g., *McGregor and Gagan*, 2004]. The relationship between the two measures of ENSO amplitude is examined first using modern coral and instrumental records of SST and then using a set of model simulations to calculate both NINO3.4 variability and the local ENSO-related variability of SST and precipitation at the coral site (a "pseudocoral" ENSO signal).

5.1. Modern Coral and Instrumental SST

[25] Observed SST from the Hadley Centre sea ice and sea surface temperature (HadISST) data set [*Rayner et al.*, 2003] and the modern coral record from Madang [*Tudhope et al.*, 2001] are used to estimate the relationship between changes in ENSO timescale variability in NINO3.4 SSTs and coral $\delta^{18}O$ over the instrumental period. We take running 20 year segments of the Madang coral record and NINO3.4 SST anomalies calculated from HadISST data for the period 1881–1992, with an offset of 2 years between segments, and calculate the standard deviation of interannual variability in the coral oxygen isotope and NINO3.4 SST seasonal anomalies. To ensure that the ENSO variability is isolated, we use a 2.5–7 year bandpass filter to smooth the seasonal coral and NINO3.4 values, following *Tudhope et al.* [2001]. Similar results were found when a 5 year offset between segments was used (not shown).

[26] The standard deviation of coral isotope anomalies is plotted against the standard deviation of NINO3.4 SST anomalies for each 20 year segment in Figure 4. In general, larger NINO3.4 SST variability is associated with larger coral $\delta^{18}O$ variability, in qualitative agreement with previous studies. Linear regression of normalized coral isotope standard deviation on normalized NINO3.4 standard deviation results in a slope of 0.68 ($r^2 = 0.70$) when only data from the period after 1920 are considered (black dots in Figure 4), whereas there is a much larger scatter for data from the 1881–1920 period (red dots in Figure 4). This implies that there may have been a change in the relationship between coral $\delta^{18}O$ variance and NINO3.4 variance in this earlier period. Alternatively, the larger scatter of data for the pre-1920 period may reflect less reliable instrument-based SST reconstructions because of scarce observations in the tropical Pacific in the early twentieth century. As the range of ENSO amplitudes sampled in the instrumental period is relatively small, coupled model simulations are used to extend the analysis to a larger range of ENSO amplitudes, comparable to the mid-Holocene change in ENSO amplitude inferred from coral proxy records.

5.2. Model Simulations

[27] A set of coupled model simulations with ENSO amplitudes that vary by more than ±50% is used to investigate the relationship between central Pacific NINO3.4 SST variability and variability of precipitation and SST at the western Pacific coral site. The simulations use standard, flux-adjusted, and perturbed physics versions of HadCM3, as described in section 3. To calculate coral $\delta^{18}O$ for the model climate, both SST and ocean water oxygen isotope ratios at the coral site are required. Previous studies have simulated ocean water oxygen isotopes by incorporating water isotope tracers into the hydrological cycle of a coupled model [*Schmidt et al.*, 2007] or by using modeled surface ocean isotope ratios and SSTs to calculate a model "coral" oxygen isotope ratio [*Brown et al.*, 2006b]. In the absence of such a water isotope tracer scheme in the current version of HadCM3, we utilize simple regression analysis to derive relationships between the variability of a pseudocoral indicator of ENSO and NINO3.4 region SST for the set of model simulations.

5.2.1. Construction of Pseudocoral

[28] The relationship between NINO3.4 SST variability and ENSO-related variability of precipitation and SST at the coral site in the western Pacific can be approximated by linear regression. Let $N34(t)$ be a time series of monthly anomalies of SST averaged in the NINO3.4 region. Given gridded observations, or the output from a model, we may solve

$$N34(t) = \beta_T T(t) + \beta_P P(t) + R(t), \quad (1)$$

where $T(t)$ is a time series of monthly SST anomalies averaged over ocean grid points in the region of the coral site, $P(t)$ is a time series of precipitation anomalies averaged in the same region, and $R(t)$ are the residuals that remain after the fit (the normal constant term is zero by construction as we are working with anomalies). We write equation (1) in this way, with the dependent and independent variables swapped in comparison with the more usual format of a regression equation, for consistency with equation (2) below. β_T and β_P are estimates of regression coefficients which capture the joint relationship between the western Pacific SST and precipitation and NINO3.4 SST. In this framework, nonzero residuals or "noise" will arise from regional fluctuations in T and P that are unrelated to ENSO as measured by the NINO3.4 index. Real coral proxies will also contain noise as a result of nonclimatic fluctuations in isotopic composition.

[29] We define a pseudocoral indicator as

$$C(t) = \beta_T T(t) + \beta_P P(t) + \sigma r(t), \quad (2)$$

where σ is the standard deviation of the residuals $R(t)$ and $r(t)$ is a series of random numbers drawn from a normal distribution with zero mean and unit variance. Thus C contains the signal of ENSO as recorded in local variations in T and P at the coral site plus some noise. Strictly speaking, we could label $C(t)$ "the reconstruction of NINO3.4 anomalies from temperature and precipitation at the coral site." The term "pseudocoral" is used because the reconstruction of NINO3.4 at the coral site is an approximation of the coral ENSO signal for the model climate.

[30] When using GCM output, it is more appropriate to average a number of grid points rather than to use single grid point values which can be contaminated with numerical noise; hence we use the region highlighted in Figure 5 which encloses PNG (approximately 144–152°E and 4–9°S). The region includes three ocean grid boxes, which is close to the minimum acceptable while retaining consistency with the point coral values. For both observations and standard flux-adjusted HadCM3, there is a negative correlation between NINO3.4 and SST and precipitation anomalies in the PNG region; that is, the region is cooler and drier during an El Niño event and warmer and wetter during a La Niña event. The use of the flux-adjusted version of the model (designated HadCM3.0) in this part of the study is crucial, as the mean SST biases that are present without flux adjustments reverse the relationship between NINO3.4 and SST and precipitation anomalies in the PNG region (Figures 5e and 5f). This is a common bias in non-flux-adjusted GCMs, many of which simulate an equatorial Pacific cold tongue that extends too far west [e.g., *AchutaRao and Sperber*, 2006].

5.2.2. Observation and Model Time Series

[31] Figure 6 shows time series of NINO3.4 and the pseudocoral indicator from observations and from HadCM3 with flux adjustments. An observational pseudocoral time series is constructed using HadISST SST data and Climate Prediction Center (CPC) merged analysis of precipitation (CMAP) [*Xie and Arkin*, 1997] and Climatic Research Unit (CRU) precipitation data (available at http://www.cru.uea.ac.uk/~mikeh/datasets/global/). The correlation between the observed NINO3.4 and pseudocoral is 0.4 when using the shorter CMAP record but falls to 0.2 when using the longer CRU record. For this longer record, contamination by random observational errors is more likely in the case of both the precipitation and PNG SST and NINO3.4 SST records. Correlations of around 0.4 are consistent with those found when correlating real coral oxygen isotope ratio anomalies with indices of ENSO, as shown in Figure 6a and reported by *Tudhope et al.* [1995, 2001].

[32] For the standard model, the correlation between NINO3.4 and the pseudocoral is higher at 0.6 (Figure 6b), which may reflect the lack of contamination by random observational or nonclimatic noise in the model output. Averaging the four PNG region grid boxes in the model may also help to boost the variance explained. Overall, the regression technique yields pseudocoral time series that are correlated with the NINO3.4 index at similar levels as seen in observations and thus explain a similar level of ENSO variability as the real coral records. In addition, the regression coefficients (Table 3) are similar for observed and model pseudocorals, indicating that the model ENSO response at the PNG site is correctly partitioned between SST and precipitation. The technique thus provides a suitable tool for assessing the relationship between coral-inferred and SST-measured ENSO variability.

[33] Using the regression coefficients from the standard HadCM3 flux-adjusted run (Table 3), we next compute pseudocoral indicators of ENSO variability from an ensemble of perturbed physics versions of HadCM3. We use 34 different preindustrial simulations and 5 simulations in which orbital parameters are set to the mid-Holocene configuration. The different model versions exhibit a wide range of ENSO amplitude and frequency characteristics compared to the standard model [*Brown et al.*, 2008; *Toniazzo et al.*, 2008]. We may consider these differences in ENSO variability to represent different epochs for which we have collected coral records and use the relationships derived from the "present day" (the standard model version) to reconstruct the characteristics of NINO3.4 variability seen in those past epochs. Figure 6c shows an example of the NINO3.4 anomalies and the pseudocoral "reconstruction" using the standard model values of β_T and β_P for a perturbed model version with low ENSO variability (designated HadCM3.3).

5.2.3. NINO3.4 SST and Pseudocoral Variability

[34] The standard deviation of seasonal anomalies of NINO3.4 SST is plotted against the standard deviation of

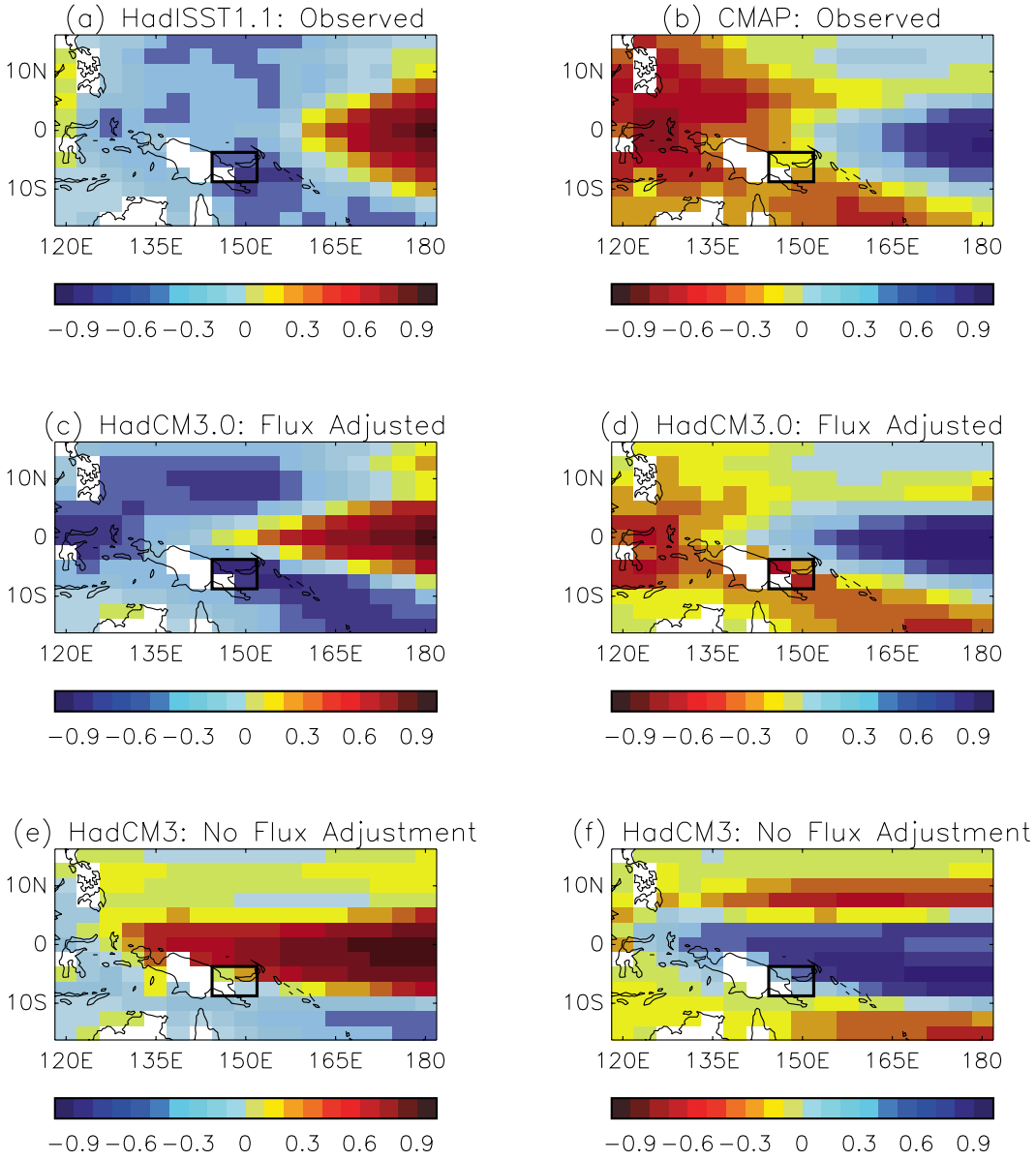

Figure 5. Spatial map of temporal correlations between monthly NINO3.4 SST anomalies and monthly SST and precipitation anomalies. (a, b) Correlations for 1979–2001 HadISST and CMAP observed records. (c, d) Correlations for flux-adjusted standard model (HadCM3.0) 100 year preindustrial runs. (e, f) Correlations for non-flux-adjusted standard model (HadCM3) 100 year preindustrial runs. The black square over PNG denotes the grid boxes used in the calculation of pseudocoral indices.

seasonal anomalies of the pseudocoral index in Figure 7. In the case of reduced NINO3.4 variability relative to the standard model, there is a corresponding reduction in pseudocoral variability. In the case of increased NINO3.4 variability, however, there is no corresponding increase in pseudocoral variability. This implies that the teleconnection has "saturated" in the sense that SSTs and precipitation in the PNG region (Figure 5) cannot attain anomalies above a certain threshold. If this relationship holds in the real climate system, corals from the western Pacific warm pool may be limited in their ability to record periods of enhanced ENSO variability in the past, although the contribution of evaporation to salinity (and $\delta^{18}O$) variability in the western Pacific is not captured by the pseudocoral indicator used here.

[35] Fitting a curve to the points in Figure 7 to obtain a quantitative estimate of the relationship between changes in coral variability and changes in NINO3.4 variability is confounded by this nonlinear relationship at high NINO3.4 variance and the relatively large spread of points. Nevertheless, by simple examination it is clear that, for example, a 20% reduction in coral standard deviation corresponds to a 30–50% reduction in NINO3.4. Therefore, the results of this model-based assessment suggest that mid-Holocene

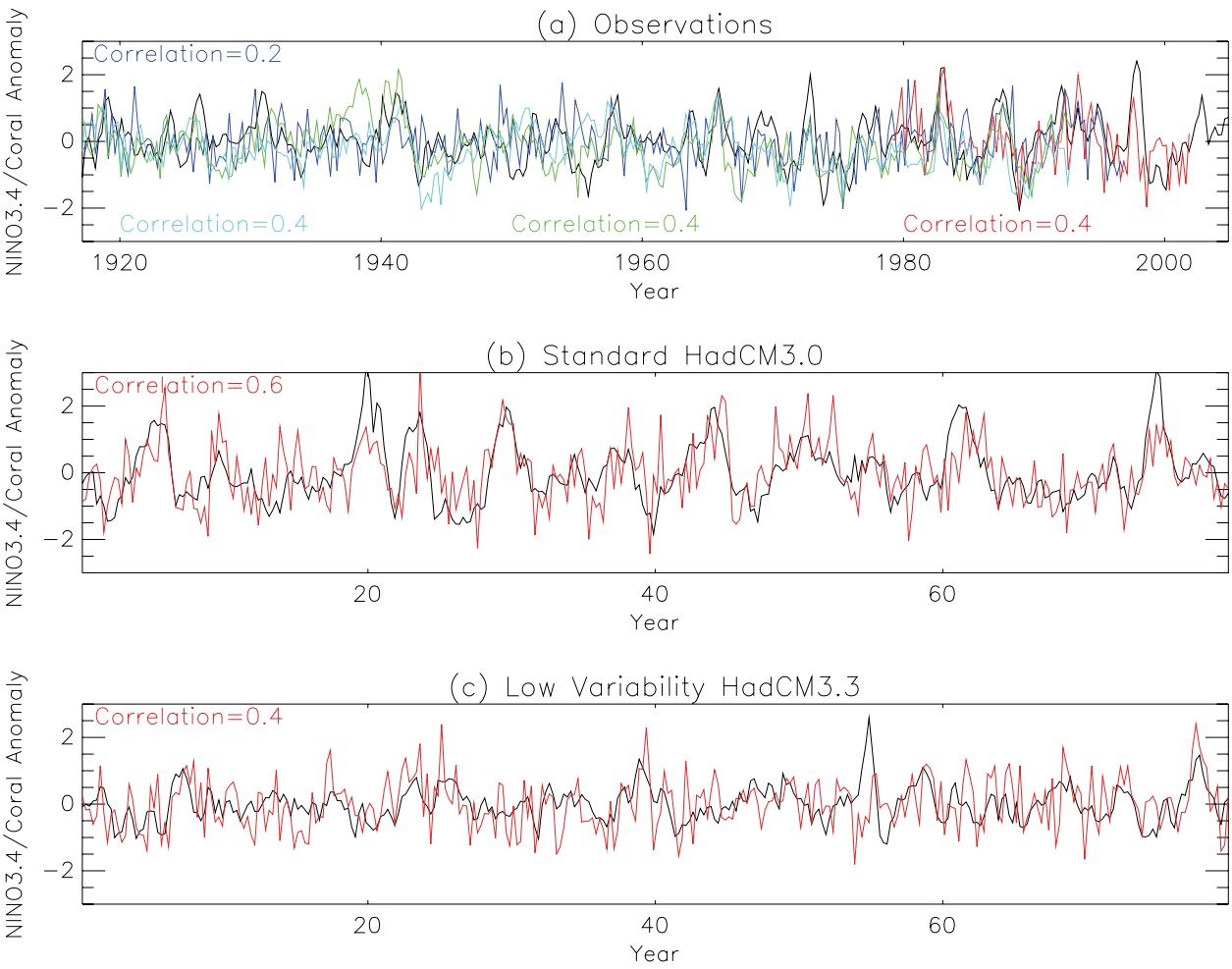

Figure 6. (a) Time series of seasonal NINO3.4 SST anomalies (black) and two pseudocoral time series computed from HadISST SST anomalies and CMAP (red) and CRU (blue) precipitation averaged over the PNG region indicated in Figure 5. Correlations between NINO3.4 and pseudocoral series are indicated in the appropriate colors. Also shown in Figure 6a are time series of coral oxygen isotope anomalies from Madang (green) and Laing (light blue) sites and associated correlations with NINO3.4 anomalies. (b) Time series of seasonal NINO3.4 anomalies (black) and pseudocoral series (red) computed from HadCM3.0 (flux-adjusted standard model). (c) As in Figure 6b but for a version of HadCM3 with reduced ENSO variability and pseudocoral time series calculated using the HadCM3.0 regression coefficients.

NINO3.4 SST variability should have been reduced by more than the ~30–60% reduction seen in PNG fossil coral records, implying an even greater discrepancy with model simulations of an ~10–15% reduction in variability.

[36] A possible explanation for the model-proxy disagreement is that the strength of ENSO precipitation or SST teleconnections in the western Pacific warm pool may have changed over the Holocene, resulting in apparent changes in ENSO amplitude recorded in corals that do not reflect changes in central Pacific SST variability. Previous studies [e.g., *Woodroffe et al.*, 2003; *Gagan et al.*, 2004; *McGregor and Gagan*, 2004] have suggested that the mechanism for the change in western Pacific ENSO teleconnection may be a northward shift of the Intertropical Convergence Zone (ITCZ) in the mid-Holocene which reduced the precipitation variability associated with ENSO over the western Pacific coral sites. While a northward shift of the Atlantic ITCZ has been inferred from changes in the composition of marine sediments in the Cariaco Basin [*Haug et al.*, 2001], it is less

Table 3. Regression Coefficients for Pseudocoral Fits to Observed and Modeled SST and Precipitation Anomalies in the PNG Region[a]

	Observed CMAP and HadISST	Observed CRU and HadISST	Standard Model
β_T (deg C/deg C)	−1.2	−1.1	−1.0
β_P (deg C/mm/d)	−0.095	−0.022	−0.069

[a]See equation (1) and associated text for more details.

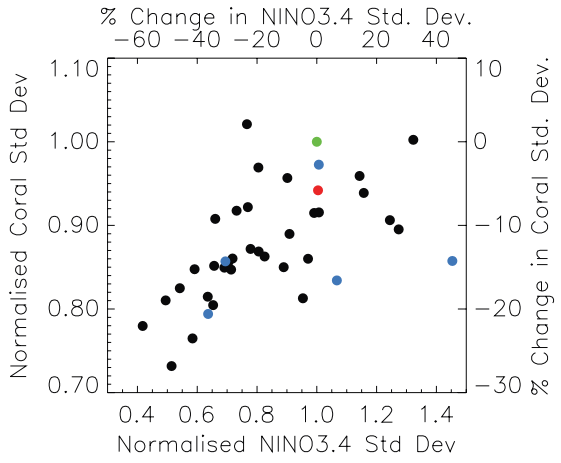

Figure 7. Standard deviation, and percentage change from standard model, of seasonal NINO3.4 SST anomalies against standard deviation of seasonal pseudocoral time series computed from several different HadCM3 simulations. The HadCM3.0 (flux-adjusted standard model) preindustrial run is shown in green, and the observed relationship from CMAP precipitation and HadISST SST is shown in red. Preindustrial perturbed physics model runs are shown in black, and mid-Holocene runs are shown in blue.

clear that a similar northward shift occurred in the western Pacific sector. There is evidence from corals and foraminifera for increased salinity in the western Pacific warm pool during the mid-Holocene [e.g., *Gagan et al.*, 2000; *Stott et al.*, 2004], in agreement with salinity and seawater oxygen isotope ratio changes simulated by a coupled model [*Schmidt et al.*, 2007]. HadCM3 mid-Holocene simulations do not show an annual mean meridional ITCZ displacement in the western Pacific, although systematic biases in the simulation of present-day climate imply that the regional mid-Holocene precipitation response may be unreliable [e.g., *Brown et al.*, 2006a, 2008]. Further model and proxy studies are needed to reconstruct the meridional position of the Pacific ITCZ in the mid-Holocene and to investigate possible impacts on regional ENSO precipitation signals.

6. Summary and Discussion

[37] We have demonstrated that four different measures of ENSO amplitude result in substantially different estimates of the reduction in ENSO amplitude in the mid-Holocene calculated from modern and fossil coral records and coupled model runs. The change in the number of events per century gives the largest percentage change for both coral records and model runs but is potentially unreliable for small numbers of events and is highly sensitive to the choice of threshold. The average El Niño event over an absolute threshold results in a reduction around half as large as the standard deviation (as expected since it measures only half of the ENSO cycle). Given the reduced number of events in the mid-Holocene records, the average event size may be biased because of the small sample size. We conclude that the standard deviation (or variance) of the anomaly time series provides a more robust measure of the full ENSO cycle, incorporating information about changes in the amplitude of both warm and cold events. By this measure, the mid-Holocene weakening of interannual variability is 57% for the Madang–Huon Peninsula corals and 27% for the Muschu Island corals.

[38] The use of monthly, seasonal, or annual average NINO3.4 SST anomalies has a large impact on the amplitude of ENSO calculated from HadCM3 model simulations. The choice of averaging period appears to be less important for the Madang–Huon Peninsula coral records, which give a similar change from modern to mid-Holocene ENSO amplitude when seasonal or annual isotopic anomalies are used. When calendar year average NINO3.4 SST anomalies are used, the standard deviation of mid-Holocene values is only 3% less than the preindustrial case. However, when July–June averages are used, the mid-Holocene ENSO amplitude is reduced by 15%. This discrepancy is explained by the tendency of El Niño events to peak at the end of the calendar year in the preindustrial simulation (and in observations), leading to a smoothing of the ENSO signal when calendar year averages are used. Using the standard deviation of July–June annual average NINO3.4 SST anomalies to measure model ENSO amplitude, the size of the change in mid-Holocene ENSO amplitude simulated by the model remains substantially smaller than the reductions estimated from the two sets of coral records.

[39] The statistical significance of changes in ENSO amplitude for records of different lengths was estimated from a 2000 year HadCM3 control simulation, and it was found that records of 100 years may sample variations in NINO3 standard deviation due to model internal variability which exceed ±20%. The exact range calculated here is only applicable to the amplitude of internal ENSO variability for HadCM3; however, a similar exercise could be carried out using subsampling of the instrumental record or modern coral records to estimate natural variability. In general, we urge caution in the interpretation of changes in past ENSO variability from short records of only a few decades since these could easily reflect sampling of natural ENSO variability rather than a response to external forcing such as orbital changes.

[40] The relationship between variability in central Pacific NINO3.4 SST and ENSO-related precipitation and SST signals in coral records from the western tropical Pacific was examined using both instrumental records and model simulations. The amplitude of interannual variability in sections of modern coral was found to increase approximately linearly with variability in the corresponding observed NINO3.4 SST anomalies from 1920 to 1992, with a larger scatter for data from 1881 to 1920. The amplitudes of variability in pseudocoral records constructed from model SST and precipitation and variability in NINO3.4 SST from the same simulations were also found to follow an approximately linear relationship. The slope of the relationship, implying greater percentage changes in model NINO3.4 variability than pseudocoral variability, does not assist in resolving the model-coral proxy disagreement identified in this study. However, the mechanisms producing varying

ENSO amplitudes amongst the perturbed physics model runs differ from the mechanisms forcing changes in ENSO amplitude over the Holocene (changes in the seasonal distribution of insolation). The relationship between coral and NINO3.4 SST variability may also have changed under mid-Holocene conditions, and possible changes in the western Pacific ENSO signal and ITCZ location require further investigation. The use of multiple (atmosphere and ocean) ENSO indices may provide a more robust basis for comparison with local paleo-ENSO records [e.g., *Gergis and Fowler*, 2005].

[41] In conclusion, this study confirms the disagreement between the reduction in the amplitude of mid-Holocene ENSO variability inferred from coral records from PNG and the reduction calculated from coupled model simulations. The use of a consistent measure of ENSO amplitude, the standard deviation of interannual variability, allows the model-proxy disagreement to be clearly identified. However, a quantitative comparison between model and coral ENSO amplitudes is limited by remaining uncertainty about the slope of the relationship under paleoclimate conditions. Obtaining mid-Holocene fossil coral records from other centers of ENSO activity is a priority to help to reduce this uncertainty. In future model-proxy comparisons, model simulations should be used to calculate changes in ENSO teleconnections at the proxy site to investigate whether the local ENSO response is invariant under paleoclimate conditions. The use of a multimodel ensemble or a perturbed physics ensemble can help to reduce the impact of systematic model biases in the simulation of ENSO teleconnections. Comparison of multiple proxy records and multiple long model simulations is necessary to ensure that changes in ENSO amplitude are not due to natural or internal multidecadal variability. Finally, if climate models remain unable to simulate the magnitude of reduction in mid-Holocene ENSO inferred from coral proxy records, we must consider the possibility that the models lack the necessary physical processes or resolution to capture the response to mid-Holocene orbital forcing. If this is the case, by implication they may also underestimate changes in ENSO variability due to anthropogenic climate change.

[42] **Acknowledgments.** We thank Amy Clement, Axel Timmermann, and David Battisti for useful discussions on aspects of this study. We also acknowledge the Hadley Centre Quantifying Uncertainty in Model Predictions (QUMP) team for providing the perturbed physics HadCM3 simulations. The comments of two anonymous reviewers greatly improved this manuscript. This study was funded by the Natural Environment Research Council (UK) RAPID program.

References

AchutaRao, K., and K. R. Sperber (2006), ENSO simulation in coupled ocean-atmosphere models: Are the current models any better?, *Clim. Dyn.*, *27*, 1–15, doi:10.1007/s00382-006-0119-7.

Ayliffe, L. K., M. I. Bird, M. K. Gagan, P. J. Isdale, H. Scott-Gagan, B. Parker, D. Griffin, M. Nongkas, and M. T. McCulloch (2004), Geochemistry of coral from Papua New Guinea as a proxy for ENSO ocean-atmosphere interactions in the Pacific warm pool, *Cont. Shelf Res.*, *24*, 2343–2356.

Braconnot, P., et al. (2007), Results of PMIP2 coupled simulations of the mid-Holocene and Last Glacial Maximum—part 1: Experiments and large-scale features, *Clim. Past*, *3*, 261–277.

Brown, J., M. Collins, and A. Tudhope (2006a), Coupled model simulations of mid-Holocene ENSO and comparisons with coral proxy records, *Adv. Geosci.*, *6*, 29–33.

Brown, J., I. Simmonds, and D. Noone (2006b), Modeling δ^{18}O in tropical precipitation and the surface ocean for present-day climate, *J. Geophys. Res.*, *111*, D05105, doi:10.1029/2004JD005611.

Brown, J., M. Collins, A. Tudhope, and T. Toniazzo (2008), Modelling mid-Holocene tropical climate and ENSO variability: Towards constraining predictions of future change with palaeo-data, *Clim. Dyn.*, *30*, 19–36, doi:10.1007/s00382-007-0270-9.

Bush, A. B. G. (1999), Assessing the impact of mid-Holocene insolation on the atmosphere-ocean system, *Geophys. Res. Lett.*, *26*, 99–102.

Cane, M. A., A. Clement, M. K. Gagan, L. K. Ayliffe, and A. W. Tudhope (2000), ENSO through the Holocene as depicted in corals and a model simulation, *PAGES Newsl.*, *8*(1), 3–7.

Clement, A. C., R. Seager, and M. A. Cane (2000), Suppression of El Niño during the mid-Holocene by changes in the Earth's orbit, *Paleoceanography*, *15*, 731–737.

Clement, A., M. Cane, and R. Seager (2001), An orbitally driven tropical source for abrupt climate change, *J. Clim.*, *14*, 2369–2375.

Collins, M., S. F. B. Tett, and C. Cooper (2001), The internal climate variability of HadCM3, a version of the Hadley Centre coupled model without flux adjustments, *Clim. Dyn.*, *17*, 61–81.

Collins, M., B. B. Booth, G. R. Harris, J. M. Murphy, D. M. H. Sexton, and M. J. Webb (2006), Towards quantifying uncertainty in transient climate change, *Clim. Dyn.*, *27*, 127–147, doi:10.1007/s00382-006-0121-0.

Gagan, M. K., L. K. Ayliffe, J. W. Beck, J. E. Cole, E. R. M. Druffel, R. B. Dunbar, and D. P. Schrag (2000), New views of tropical paleoclimates from corals, *Quat. Sci. Rev.*, *19*, 45–64.

Gagan, M. K., E. J. Hendy, S. G. Haberle, and W. S. Hantoro (2004), Post-glacial evolution of the Indo-Pacific warm pool and El Niño–Southern Oscillation, *Quat. Int.*, *118–119*, 127–143.

Gergis, J. L., and A. M. Fowler (2005), Classification of synchronous oceanic and atmospheric El Niño–Southern Oscillation (ENSO) events for palaeoclimate reconstruction, *Int. J. Climatol.*, *25*, 1541–1565.

Haug, G. H., K. A. Hughen, D. M. Sigman, L. C. Peterson, and U. Rohl (2001), Southward migration of the Intertropical Convergence Zone through the Holocene, *Science*, *293*, 1304–1307.

Hewitt, C. D., and J. F. B. Mitchell (1998), A fully coupled GCM simulation of the climate of the mid-Holocene, *Geophys. Res. Lett.*, *25*, 361–364.

Kitoh, A., and S. Murakami (2002), Tropical Pacific climate at the mid-Holocene and the Last Glacial Maximum simulated by a coupled ocean-atmosphere general circulation model, *Paleoceanography*, *17*(3), 1047, doi:10.1029/2001PA000724.

Liu, Z., J. Kutzbach, and L. Wu (2000), Modeling climate shift of El Niño variability in the Holocene, *Geophys. Res. Lett.*, *27*, 2265–2268.

Liu, Z., S. P. Harrison, J. Kutzbach, and B. Otto-Bliesner (2004), Global monsoons in the mid-Holocene and oceanic feedback, *Clim. Dyn.*, *22*, 157–182.

McGregor, H. V., and M. K. Gagan (2004), Western Pacific coral δ^{18}O records of anomalous Holocene variability in the El Niño–Southern Oscillation, *Geophys. Res. Lett.*, *31*, L11204, doi:10.1029/2004GL019972.

Moy, C. M., G. O. Seltzer, D. T. Rodbell, and D. M. Anderson (2002), Variability of El Niño/Southern Oscillation activity at millennial timescales during the Holocene epoch, *Nature*, *420, 162–165.*

Murphy, J., D. Sexton, D. Barnett, G. Jones, M. Webb, M. Collins, and D. Stainforth (2004), Quantification of modelling uncertainties in a large ensemble of climate change simulations, *Nature*, *430*, 768–772.

Otto-Bliesner, B. L., E. C. Brady, S.-I. Shin, Z. Liu, and C. Shields (2003), Modeling El Niño and its tropical teleconnections during the last glacial-interglacial cycle, *Geophys. Res. Lett.*, *30*(23), 2198, doi:10.1029/2003GL018553.

Rayner, N. A., D. E. Parker, E. B. Horton, C. K. Folland, L. V. Alexander, D. P. Rowell, E. C. Kent, and A. Kaplan (2003), Global analyses of sea surface temperature, sea ice, and night marine air temperature since the late nineteenth

century, *J. Geophys. Res.*, *108*(D14), 4407, doi:10.1029/2002JD002670.

Riedinger, M. A., M. Steinitz-Kannan, W. M. Last, and M. Brenner (2002), A ~6100 ^{14}C yr record of El Niño activity from the Galápagos Islands, *J. Paleolimnol.*, *27*, 1–7.

Rodbell, D. T., G. O. Seltzer, D. M. Anderson, M. B. Abbott, D. B. Enfield, and J. H. Newman (1999), An ~15,000 year record of El Niño-driven alluviation in southwestern Ecuador, *Science*, *283*, 516–520.

Schmidt, G. A., A. N. LeGrande, and G. Hoffmann (2007), Water isotope expressions of intrinsic and forced variability in a coupled ocean-atmosphere model, *J. Geophys. Res.*, *112*, D10103, doi:10.1029/2006JD007781.

Stott, L., K. Cannariato, R. Thunell, G. H. Haug, A. Koutavas, and S. Lund (2004), Decline of surface temperature and salinity in the western tropical Pacific Ocean in the Holocene epoch, *Nature*, *431*, 56–59.

Toniazzo, T., M. Collins, and J. Brown (2008), The variation of ENSO characteristics associated with atmospheric parameter perturbations in a coupled model, *Clim. Dyn.*, *30*, 643–656, doi:10.1007/s00382-007-0313-2.

Trenberth, K. (1997), The definition of El Niño, *Bull. Am. Meteorol. Soc.*, *78*, 2771–2777.

Tudhope, A. W., G. B. Shimmield, C. P. Chilcott, M. Jebb, A. Fallick, and A. Dalgleish (1995), Recent changes in climate in the far western equatorial Pacific and their relationship to the Southern Oscillation; oxygen isotope records from massive corals, Papua New Guinea, *Earth Planet. Sci. Lett.*, *136*, 575–590.

Tudhope, A. W., C. P. Chilcott, M. T. McCulloch, E. R. Cook, J. Chappell, R. M. Ellam, D. W. Lea, J. M. Lough, and G. B. Shimmield (2001), Variability in the El Niño–Southern Oscillation through a glacial-interglacial cycle, *Science*, *291*, 1511–1517, doi:10.1126/science.1057969.

Woodroffe, C. D., M. R. Beech, and M. K. Gagan (2003), Mid-late Holocene El Niño variability in the equatorial Pacific from coral microatolls, *Geophys. Res. Lett.*, *30*(7), 1358, doi:10.1029/2002GL015868.

Xie, P., and P. A. Arkin (1997), Global precipitation: A 17-year monthly analysis based on gauge observations, satellite estimates, and numerical model outputs, *Bull. Am. Meteorol. Soc.*, *78*, 2539–2558.

J. Brown, School of Geography and Environmental Science, Monash University, Clayton, Vic 3800, Australia. (josephine.brown@arts.monash.edu.au)

M. Collins, Hadley Centre for Climate Prediction and Research, Met Office, Exeter EX1 3PB, UK.

H. V. McGregor, School of Earth and Environmental Sciences, University of Wollongong, Wollongong, NSW 2522, Australia.

A. W. Tudhope, School of Geosciences, University of Edinburgh, Edinburgh EH8 9YL, UK.